American Mineralogist, Volume 65, pages 867-884, 1980

Structure and redox equilibria of iron-bearing silicate melts

BJØRN O. MYSEN, FRIEDRICH SEIFERT[1] AND DAVID VIRGO

Geophysical Laboratory, Carnegie Institution of Washington
Washington, D.C. 20008

Abstract

Redox equilibria and coordination states of iron in silicate melts have been determined with Mössbauer spectroscopy. The anionic structure of the silicate network of the melts has been determined with laser Raman spectroscopy.

Mössbauer spectroscopic data indicate that in all quenched melts in the system Na_2O–FeO–Fe_2O_3–SiO_2 at 1 atm pressure, ferric iron is in tetrahedral coordination, probably as an $NaFeO_2$ complex. For example, melt of $NaFe^{3+}Si_2O_6$ composition quenched from 1400°C has a three-dimensional network structure. In all melts, the Fe^{2+} is octahedrally coordinated with oxygen.

Both Fe^{3+} and Fe^{2+} are network modifiers in the system CaO–MgO–FeO–Fe_2O_3–SiO_2, probably because $CaFe_2O_4$ and $MgFe_2O_4$ complexes are not stable in molten silicates. Only alkali metals can stabilize ferric iron in tetrahedral coordination.

Quenched melts along joins such as Na_2SiO_3–$NaFeSi_2O_6$ become progressively more polymerized as the acmite content of the system increases. Under $f(O_2)$ conditions more reducing than that of air, $Fe^{2+}/\Sigma Fe$ of the melts also increases with increasing acmite content (increasing degree of polymerization) of the melt. At fixed bulk composition iron-bearing melts of alkali silicates become depolymerized with decreasing $f(O_2)$ because $NaFeO_2$ complexes in the silicate network are transformed to $Fe^{2+}O_6^{10-}$ octahedra, whereby ferrous iron becomes a network modifier.

The Raman spectra are interpreted to suggest that the anionic structure of quenched metasilicate melts on the join $CaSiO_3$–$MgSiO_3$ predominantly consists of three structural units—separate SiO_4^{4-} tetrahedra, $Si_2O_5^{2-}$ and $Si_2O_6^{4-}$ units. The proportions of SiO_4^{4-} and $Si_2O_5^{2-}$ units increase relative to that of $Si_2O_6^{4-}$ units as the Ca/(Ca + Mg) of the melt increases. In melts on this join with 5 mole % $FeSiO_3$ component added, the $Fe^{2+}/\Sigma Fe$ decreases with increasing Ca/(Ca + Mg). This decrease is related to the increased degree of proportionation of the $Si_2O_6^{4-}$ units to SiO_4^{4-} and $Si_2O_5^{2-}$ units with increasing Ca/(Ca + Mg).

Provided that sufficient alkali metal is available in rock-forming silicate melts for local charge balance of Fe^{3+}, the ferric iron will be in the network. A progressive decrease of M^+/M^{2+} of a magma (as a result of fractional crystallization, for example) will result in ferric iron shifting from IV to VI coordination, thus changing the anionic structure of the melt. This change will also change some properties of the melt such as viscosity and density and the activity coefficients of trace elements.

Introduction

The redox ratio of iron in rock-forming silicate melts is often used as an indicator of petrogenetic history (*e.g.*, Fudali, 1965). Its partitioning behavior between melts and crystals has also been used to deduce the petrogenetic history of basaltic and derivative melts (Osborn, 1959, 1962, 1977; Carmichael, 1967; Buddington and Lindsley, 1964; Roeder and Emslie, 1970).

Recent experimental work has been devoted to determining the influence of both intensive and extensive variables on the redox ratio of iron in silicate melts (Lauer, 1977; Lauer and Morris, 1977; Schreiber *et al.*, 1978; Mysen and Virgo, 1978). The problem is complex because iron may not simply respond to variations in melt structure; rather it may affect

[1] Present address: Mineralogisch-Petrographisches Institut und Museum der Universität Kiel, Olshaussenstrasse 40–60, 2300 Kiel, West Germany.

0003–004X/80/0910–0867$02.00

the melt structure in important ways. Furthermore, the iron component in a melt can play a dual role because Fe can be both tetrahedrally and octahedrally coordinated. The structural role of iron is controlled by an involved interrelationship between degree of polymerization of the host, types of cations present, amount of iron present and its oxidation state (Waff, 1977). In an attempt to understand these problems, a study of the anionic structure of quenched Fe-bearing silicate melts has been undertaken. In this report the structural role of iron as a function of oxygen fugacity and bulk composition of the melt is emphasized.

Experimental techniques

Bulk compositions were chosen to determine the relations between redox states of iron and the ratio of nonbridging to bridging oxygen in the melt (NBO/BO) and the effect of different modifying cations on the structural role of ferric and ferrous iron. Such an effect is most conveniently studied in systems like Na_2O–FeO–Fe_2O_3–SiO_2(NFFS) and CaO–MgO–FeO–Fe_2O_3–SiO_2 (CMFFS) because structural data on melts in portions of these systems are already available (Brawer and White, 1975, 1977; Etchepare, 1972; Brown *et al.*, 1978; Mysen and Virgo, 1978, in preparation; Seifert *et al.*, 1979a,b; Mysen *et al.*, 1979; Virgo *et al.*, 1980). The NBO/BO varies as a systematic function of Na content of melts on the join Na_2O–SiO_2, for example (Brawer and White, 1975). It is also known that the anionic structure of quenched metasilicate melts is similar for a larger variety of network-modifying cations (Brawer and White, 1975, 1977; Verweij and Konijnendijk, 1976; Virgo *et al.*, 1980; Mysen *et al.*, 1980).

The starting materials were prepared from spectroscopically pure (Johnson and Matthey) SiO_2, Fe_2O_2, MgO, $CaCO_3$, and reagent grade Na_2CO_3.

The mixtures, (10–30 mg) were held at 1400–1585°C as beads on the Pt-wire loops in air or in a gas mixing furnace for time periods ranging from 6 to 1/2 hr, depending on the temperature of the experiment. Mysen and Virgo (1978) determined redox ratios of iron in melts on the join $NaAlSi_2O_6$–$NaFe^{3+}Si_2O_6$ as a function of time at 1450°C, and found that at that temperature a sample of about 50 mg would equilibrate with the surrounding atmosphere in about 1/2 hr. The present samples generally are less viscous than those studied by Mysen and Virgo. It is likely, therefore, that >1/2 hr run durations are sufficient to attain equilibrium.

The samples are quenched in air, mercury, or liquid nitrogen to produce glasses of the appropriate compositions. The compositions given here are nominal values.

The Mössbauer spectroscopic techniques were identical with those of Mysen and Virgo (1978). Except for the magnetic spectra (see below), a maximum of three lines were visually resolved when both ferric and ferrous iron were present in the quenched glasses, and only up to three lines of Lorentzian shape were fitted to the spectra. The absence of any splitting or even significant broadening of the low-velocity line indicates that the position of the low-velocity component of the ferric doublet closely matches that of the low-velocity component of the ferrous doublet, so that the sum of these two lines can be treated numerically as a single line. Further justification for this procedure can be derived from the position of the low-velocity line in largely ferrous and completely ferric samples. For instance, in glass of acmite composition the velocity changes from −0.132 mm/sec (relative to metallic iron) in the reduced sample to −0.237 mm/sec in the oxidized sample, a small change compared with the half-width of these absorption lines (about 0.60 mm/sec).

The $Fe^{2+}/\Sigma Fe$ values have been calculated from the area ratios of the ferrous and ferric doublets (see also Mysen and Virgo, 1978). When only two lines (due to the ferrous doublet) can be observed, any deviation of the $Fe^{2+}/\Sigma Fe$ value from 1 will be reflected in the inequality of peak areas. An example of this effect is the relation between $f(O_2)$ and $Fe^{2+}/\Sigma Fe$, as discussed further below. The $Fe^{2+}/\Sigma Fe$ is calculated from the difference of the peak areas. The reliability of $Fe^{3+}/\Sigma Fe$ of glasses determined with Mössbauer spectroscopy was discussed in some detail by Mysen and Virgo (1978), who also reported comparative studies using wet-chemical analysis as an additional technique. Comparative studies using wet-chemical and Mössbauer techniques for determination of $Fe^{3+}/\Sigma Fe$ were also conducted by Bancroft and Burns (1969) and Bancroft *et al.* (1969). In those studies, there generally was agreement between the results with the two methods. Whenever discrepancies arose, the wet-chemical technique gave higher $Fe^{3+}/\Sigma Fe$. Replicate wet-chemical analysis of such samples brought the results into agreement. It should be mentioned in this context that the wet-chemical techniques used are oxidation techniques. It is not surprising, therefore, that if there are discrepancies, they tend to be on the side of too much ferric iron. Kurkjian (1970) used published redox ratios of iron-bearing glasses on the join Na_2O–SiO_2–

FeO–Fe_2O_3 based on wet-chemical analysis (where no report on technique for wet-chemical analysis is given) and compared the results from those uncharacterized samples with Mössbauer results obtained by him on a new set of samples. In that study, results with both higher and lower $Fe^{3+}/\Sigma Fe$ values were reported. Inasmuch as the samples used in that study were not described appropriately, one cannot assess the quality of either the wet-chemical or the Mössbauer results. Therefore, the conclusions drawn by Kurkjian (1970) are open to question.

The Raman spectra were taken on small chips of quenched melts (~ 0.5–1.0 mm cubes) that were free of bubbles. The spectra were recorded with a Jobin–Yvon optical system, holographic grating, double monochromator (HG25), and a photon-counting detection system. The spectra were recorded at about 3 cm^{-1}/sec. The iron-free samples were excited with the 488.0 nm line of an Ar^+ laser, using a laser power of 200–400 mW at the sample with a 90° scattering geometry. The iron-bearing samples were excited with the 647.1 nm line of the Kr^+ ion laser also operated at 200–400 mW. Polarized spectra were obtained with the focused exciting beam parallel to the horizontal spectrometer slit and with the electric vector of the exciting radiation in a vertical orientation. A sheet of polarizer disk in front of an optical scrambler was used to record separately the parallel and perpendicular components of the scattered radiation.

As a matter of routine, replicate spectra from the same chips, from different chips of the same experimental run product, and from replicate experimental run products were also taken.

Results and discussion

Mössbauer spectroscopy

The hyperfine parameters calculated from the Mössbauer data on quenched melts in the system Na_2O–FeO–Fe_2O_3–SiO_2 are shown in Table 1. Spectra of crystalline acmite, composition $NaFe^{3+}Si_2O_6$ (Bowen *et al.,* 1930) and a ferrous-bearing akermanite (50 mole percent FeAk–50 mole percent Ak) were also taken (Table 2), in order to determine the hyperfine parameters for ferric iron in octahedral coordination and ferrous iron in tetrahedral coordination.

In all quenched melts on the join Na_2SiO_3–$NaFe^{3+}Si_2O_6$ (NS–Ac) in air, the absence of any absorption peak at about 1.8 mm/sec and the equal intensity and half-width of the two-component peaks of the doublet indicate that more than 95 percent of the iron is in the ferric state (Fig. 1). In quenched melts with 6 mole percent or less Ac (NS94Ac6), an additional line is observed at about 1.5 mm/sec (Fig. 2) and the tail region of the envelope extends to at least 7.5 mm/sec. In spectra taken at 77K (Fig. 2B) individual lines appear in this tail region, which constitutes a broadened magnetic sextet pattern superimposed on a doublet. The magnetic splitting supposedly arises from long relaxation times of spin–spin interactions of Fe^{3+} at these low iron concentrations (Bhargava *et al.*, 1979).

Table 1. Hyperfine parameters of ferric iron of quenched melts on the join Na_2SiO_3–$NaFe^{3+}Si_2O_6$ at 1400°C in air (mm/sec)

Composition	IS(Fe^{3+})	QS(Fe^{3+})
NS85Ac15	0.264	0.847
NS75Ac25	0.232	0.832
NS50Ac50	0.227	0.732
NS25Ac75	0.249	0.906
Ac100	0.249	0.971

IS(Fe^{3+}), isomer shift of Fe^{3+} relative to metallic iron. QS(Fe^{3+}), quadrupole splitting of Fe^{3+}.

The quenched melts on the join NS–Ac with more than 6 mole percent acmite component but with $Na_2O < SiO_2$, quenched in air, show similar features. We conclude, therefore, that all iron is in the ferric state (within the detection limit, <95%) in the melts in the system Na_2O–Fe_2O_3–SiO_2 when equilibrated in air.

The Mössbauer spectra of the melts in the system Na_2O–Fe_2O_3–SiO_2 show a visually resolved doublet (Fig. 1) with isomer shifts in the range between 0.23 and 0.26 mm/sec and quadrupole splitting from 0.79 to 0.97 mm/sec (Table 1). These values compare with isomer shift values of 0.38–0.40 mm/sec and quadrupole splitting of 0.30 mm/sec, respectively, for the two crystalline phases with Fe^{3+} in octahedral coordination (Fig. 1; see also Table 2).

Only compositions with small amounts of sodium metasilicate component have been investigated at low oxygen fugacity because of excessive sodium loss from the depolymerized melts close to the Na_2SiO_3 composition (Seifert *et al.*, 1979a). Even in the more Si- and Fe-rich compositions some loss of sodium to the CO_2/CO vapor phase of the furnace may have taken place, and the compositions studied may therefore not lie exactly on the join.

As the oxygen fugacity is lowered, the ferric doublet in the Mössbauer spectra becomes asymmetric, and eventually a new line at ~1.8mm/sec is ob-

Table 2. Hyperfine parameters of iron-bearing crystalline materials (mm/sec)

Composition	IS(Fe^{3+})	IS(Fe^{2+})	QS(Fe^{3+})	QS(Fe^{2+})
$NaFe^{3+}Si_2O_6$	0.399	...	0.301	...
$Na_5Fe^{3+}Si_4O_{12}$	0.377	...	0.300	...
$(CaFe^{2+}_2Si_2O_7)_{50\ mole\ \%}(CaMg_2Si_2O_7)_{50\ mole\ \%}$	...	0.958	...	2.394

IS(Fe^{3+}), isomer shift of Fe^{3+} relative to Fe metal. IS(Fe^{2+}), isomer shift of Fe^{2+} relative to Fe metal QS(Fe^{3+}), quadrupole splitting of Fe^{3+}. QS(Fe^{2+}), quadrupole splitting of Fe^{2+}.

served. The intensity of this new line increases as the oxygen fugacity decreases (Fig. 3). Concomitantly, the intensity of the high-velocity component of the ferric doublet decreases until only two lines of nearly equal area are observed (Fig. 3, Table 3), as also discussed above. The low-velocity component of this doublet is more intense and has smaller line width than the high-velocity component. The isomer shift of the latter doublet (~0.95 mm/sec) is typical of ferrous iron, and the $Fe^{2+}/\Sigma Fe$ values could be determined from its area, as described in the section on experimental techniques. The $Fe^{2+}/\Sigma Fe$ values thus derived show systematic relationships to both bulk composition and oxygen fugacity (Fig. 4). At constant oxygen fugacity the $Fe^{2+}/\Sigma Fe$ increases as the acmite content of the quenched melt is increased from 50 mole percent Ac toward pure acmite. At constant bulk composition the $Fe^{2+}/\Sigma Fe$ increases with decreasing oxygen fugacity.

The Mössbauer spectra of quenched melts in the system CaO–MgO–FeO–Fe_2O_3–SiO_2 are shown in Figures 5 and 6 (see also Table 4). In all samples, except the two at $MgSiO_3$ + 5 mole percent $FeSiO_3$ at 1585°C and $CaMgSi_2O_6$ + 1 mole percent $FeSiO_3$ at 1425°C, a ferric iron doublet is visually resolved. The line widths of the component peaks of the Mössbauer

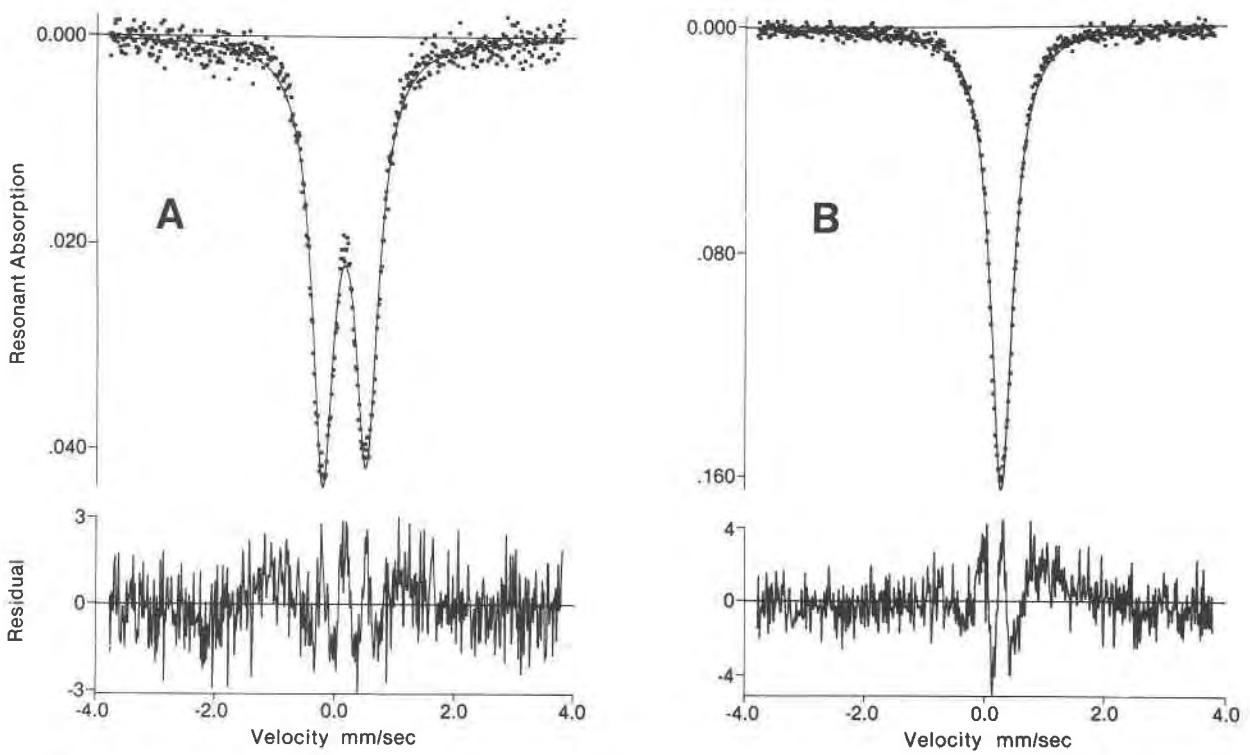

Fig. 1. ^{57}Fe Mössbauer spectra of the composition NFS518 (50 mole percent Na_2SiO_3–50 mole percent $NaFe^{3+}Si_2O_6$) in air. (A) Quenched melt. (B) Crystalline.

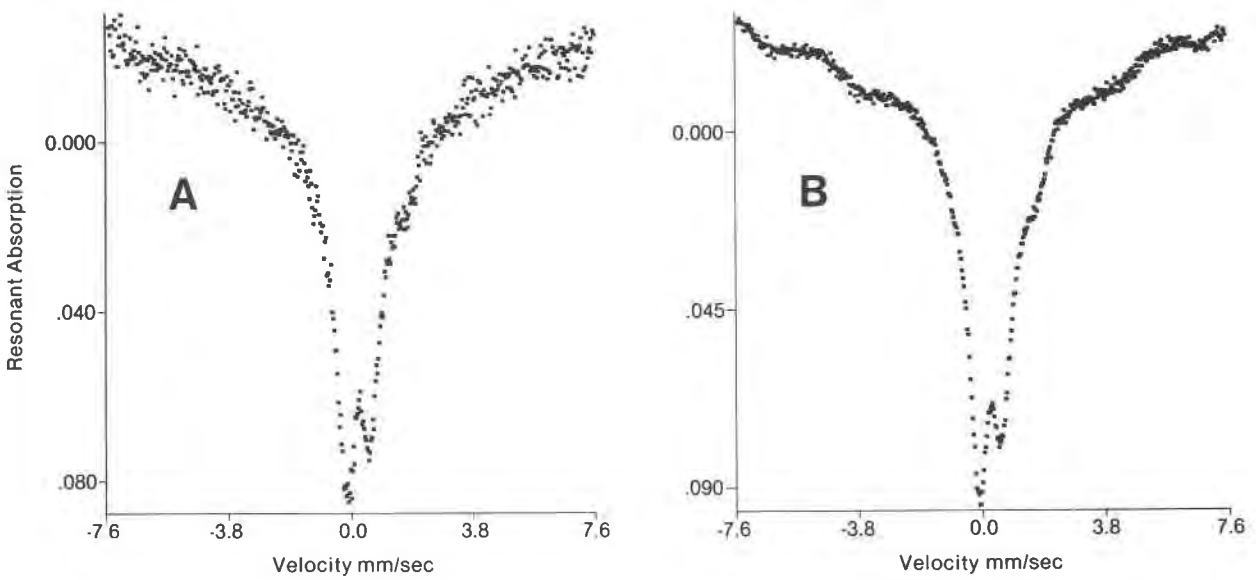

Fig. 2. ^{57}Fe Mössbauer spectra of quenched melt of Na_2SiO_3 composition with 1 mole percent $NaFe^{3+}Si_2O_6$. (A) 298K. (B) 77K.

spectra of quenched metasilicate melts of the alkaline earths are generally greater (0.8–0.9 mm/sec) than those of alkali metasilicate melts with similar amounts of iron present (0.5–0.6 mm/sec).

The isomer shift of ferric iron [IS(Fe^{3+})] of melts in the system CMFFS is greater than 0.37 mm/sec and generally greater than 0.45 mm/sec (Table 4). That of ferrous iron [IS(Fe^{2+})] is about 1 mm/sec for all compositions studied. The quadrupole splitting of ferric iron is about 1 mm/sec and that of ferrous iron is about 2 mm/sec.

The $Fe^{2+}/\Sigma Fe$ of quenched melts of alkaline earth metasilicate melts as a function of temperature and Ca/(Ca + Mg) and $FeSiO_3$ content of the starting material in air is shown in Figures 7–9. No evidence for a magnetic component was found in the Mössbauer spectra of metasilicate melts of the alkaline earths with low iron content. The $Fe^{2+}/\Sigma Fe$ of melts with 5 mole percent $FeSiO_3$ component added to the starting material increases with decreasing Ca/(Ca + Mg) in air at 1585°C (Fig. 8). Even the most oxidized sample, however, contains about 50 percent ferrous

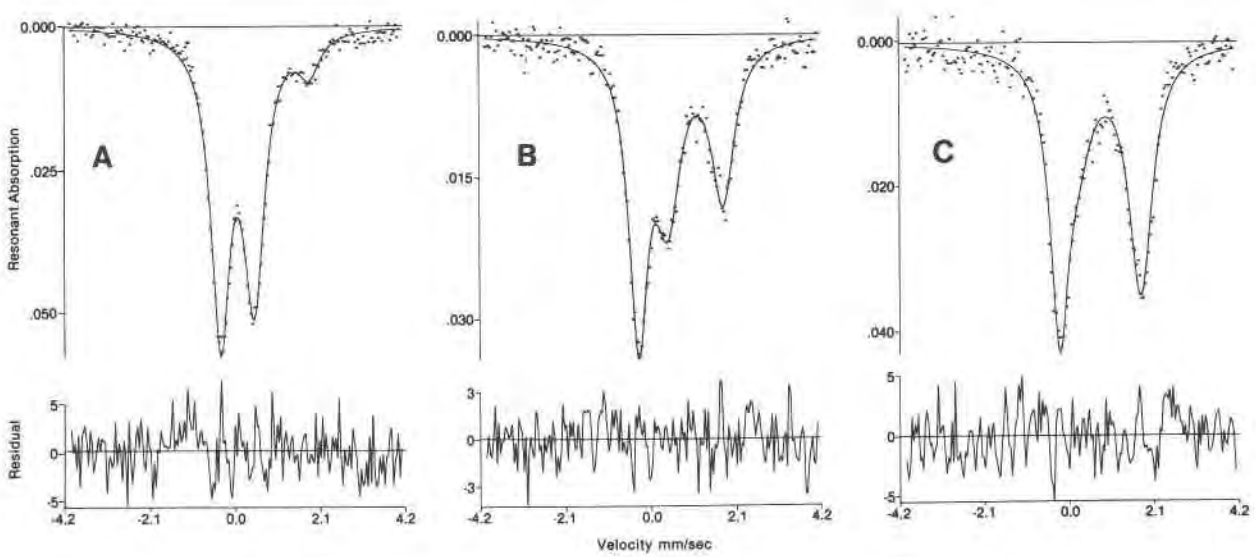

Fig. 3. ^{57}Fe Mössbauer spectra of quenched melts of composition NFS518 (see Fig. 1) as a function of $f(O_2)$ at 1400°C. (A) $f(O_2) = 10^{-4}$ atm. (B) $f(O_2) = 10^{-6}$ atm. (C) $f(O_2) = 10^{-8}$ atm.

Table 3. Hyperfine parameters and area ratios of glasses in the system sodium metasilicate–acmite–$Na_2O{\cdot}2FeO{\cdot}4SiO_2$ under reducing conditions

Composition, mole % acmite	Log $f(O_2)$, atm	Fe^{3+}				Fe^{2+}				$Fe^{2+}/\Sigma Fe$
		IS, mm/sec	QS, mm/sec	$FWHH_L$	$FWHH_H$	IS, mm/sec	QS, mm/sec	$FWHH_L$	$FWHH_H$	
50	-4	0.253	0.833	0.556	0.603	0.938	2.194		0.539	0.126
	-6	0.264	0.744	0.568	0.732	0.938	2.091		0.628	0.435
	-8	0.182	0.468	0.534	0.898	0.956	2.044		0.699	0.750
75	-4	0.260	0.879	0.583	0.591	0.925	2.209		0.592	0.117
	-6	0.283	0.759	0.609	0.720	0.940	2.060		0.696	0.505
	-8					0.991	1.955	0.755	0.754	0.889
	-10					0.993	1.943	0.681	0.746	0.916
100	-4	0.249	0.884	0.593	0.611	0.888	2.148		0.811	0.228
	-6	0.302	0.691	0.618	0.699	0.956	2.033		0.722	0.656
	-8					0.937	1.937	0.682	0.787	0.927

The compositions are given in terms of the oxidized system.
IS, isomer shift relative to metallic iron. QS, quadrupole splitting. FWHH, full width at half height. Indices H and L, high- and low-velocity component peaks.

iron. The $Fe^{2+}/\Sigma Fe$ also increases with increasing temperature (Fig.9). We also noted that at similar temperature, oxygen fugacity, and iron content, about 50 percent of the iron is ferrous in quenched matasilicate melts of the alkaline earths whereas all the iron is ferric in sodium metasilicate melts (Figs. 4 and 9).

The structural role of iron in the quenched melts can be determined to a large extent from its coordination to oxygen, which is reflected by the hyperfine parameters of the Mössbauer spectra. Tetrahedral and octahedral Fe^{3+} show well-defined ranges of isomer shifts in crystalline phases (0.19–0.30 mm/sec and 0.36–0.50 mm/sec, respectively; Annersten and Hålenius, 1976; Kurkjian, 1970; Taneja *et al.*, 1973; Annersten and Olesch, 1978). The isomer shifts observed for Fe^{3+} in the quenched melts of sodium metasilicate–acmite composition (about 0.25 mm/sec) are therefore typical of ferric iron in tetrahedral coordination. In addition, the rather sharp lines and the absence of any distinct asymmetry preclude the existence of significant amounts of octahedral Fe^{3+}. Further support for this interpretation is found in the large difference in IS(Fe^{3+}) of melts and crystals of $NaFe^{3+}Si_2O_6$ and $Na_5Fe^{3+}Si_4O_{12}$ compositions (0.23–0.26 mm/sec and 0.38–0.40 mm/sec, respectively; Tables 1 and 2). Note that Brown *et al.* (1978) concluded that the Fe^{3+} is in tetrahedral coordination, based on EXAFS analysis.

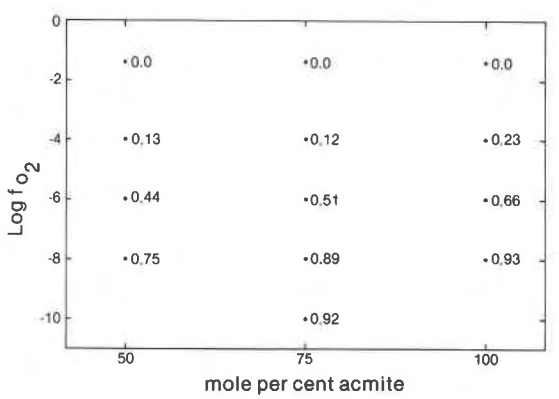

Fig. 4. $Fe^{2+}/\Sigma Fe$ of melts on the join Na_2SiO_3–$NaFe^{3+}Si_2O_6$ at 1400°C as a function of $f(O_2)$ and acmite component.

The isomer shifts of alkaline-earth metasilicate melts for ferric iron are generally in the range of 0.45–0.50 mm/sec (Table 4), which is well within the range of IS(Fe^{3+}) of ferric iron in octahedral coordination in crystalline materials (Annersten and Hålenius, 1976; Annersten and Olesch, 1978; see also Mysen and Virgo, 1978). We conclude, therefore, that tetrahedrally-coordinated ferric iron is unstable relative to octahedrally-coordinated ferric iron in quenched alkaline-earth metasilicate melts.

The hyperfine parameters of ferrous-iron quenched melts apparently are less sensitive to oxygen coordination number than those of ferric iron. In crystalline ferrous akermanite (50 mole percent)–akermanite (50 mole percent), the IS(Fe^{2+}) is about 0.95 mm/sec and the quadrupole splitting is about 2.35 mm/sec.

The isomer shifts of ferrous iron in the present quenched melts are between that of octahedral (generally greater than 1.10 mm/sec) and tetrahedral (about 0.90 mm/sec) ferrous iron in crystalline com-

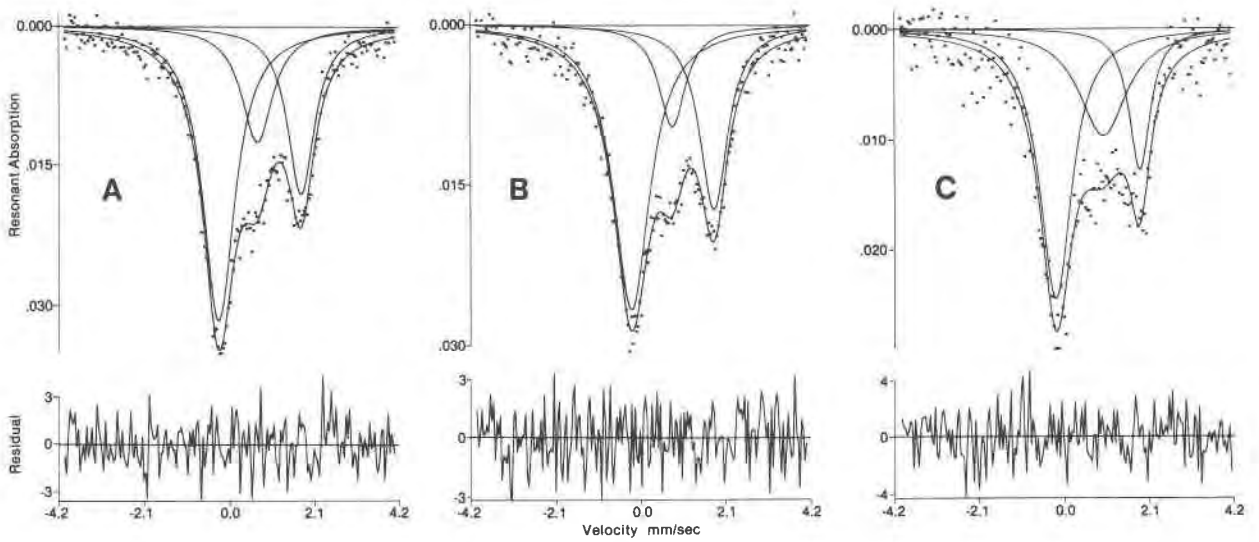

Fig. 5. ^{57}Fe Mössbauer spectra of quenched melts on the join $CaSiO_3$–$MgSiO_3$ with 5 mole percent $FeSiO_3$ component at 1585°C and 1 atm in air. (A) $CaSiO_3$. (B) $CaMgSi_2O_6$. (C) $MgSiO_3$.

pounds. Octahedral ferrous iron seems to exhibit systematically lower isomer shifts in quenched melts compared with crystals, however, as exemplified by the isomer shift of Fe^{2+} in synthetic quenched melts (1.04–1.07 mm/sec) where Fe^{2+} is known to occupy octahedral positions from optical absorption studies (Mao *et al.*, 1973; Bell and Mao, 1974).

These low values might be related to the decrease of the IS(Fe^{2+}) with increasing distortion of the octahedron (Seifert and Olesch, 1977). The quadrupole splitting of Fe^{2+} also indicates distorted sites.

We conclude, therefore, that at least a major fraction of ferrous iron in the quenched melts we studied is incorporated into octahedral positions. Ferric iron is in tetrahedral coordination in quenched melts with alkali metals. In quenched melts in which alkaline earths are the dominant modifying components, ferric iron is in octahedral coordination. Ferrous iron is in octahedral coordination in both types of melts.

Raman spectroscopy

In order to provide a framework for band-assignments in the melts under consideration, the Raman

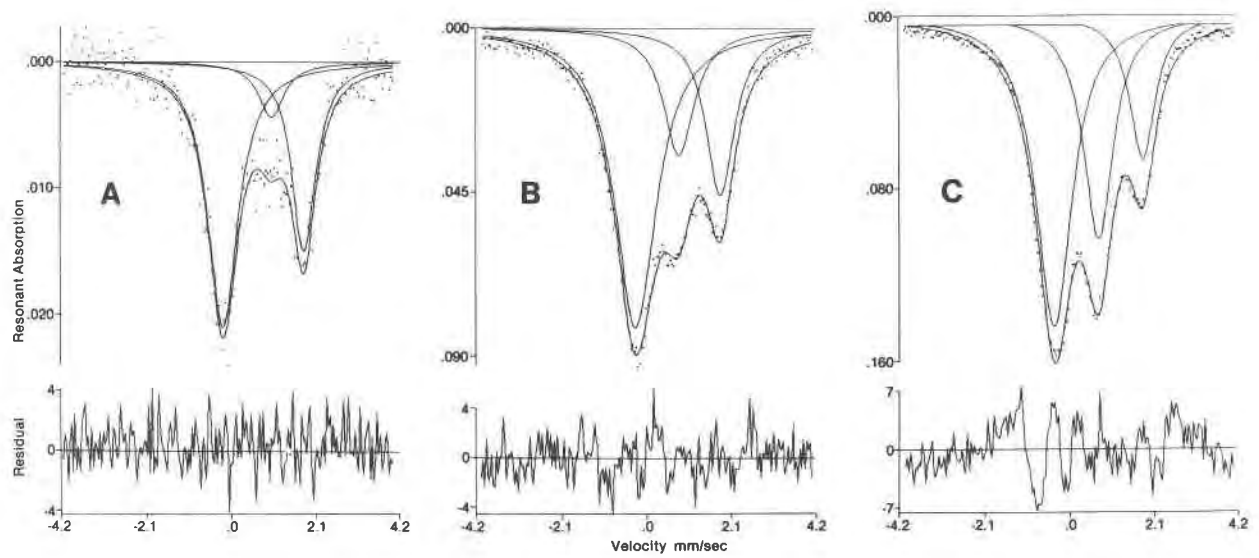

Fig. 6. ^{57}Fe Mössbauer spectra of quenched melts on the join $CaMgSi_2O_6$–$FeSiO_3$ at 1425°C and 1 atm in air. (A) 1 mole percent $FeSiO_3$. (B) 5 mole percent $FeSiO_3$. (C) 10 mole percent $FeSiO_3$.

Table 4. Mössbauer data on quenched melts in the system $CaO–MgO–FeO–Fe_2O_3–SiO_2$

Composition	Temp., °C	$f(O_2)$	Fe^{3+}		Fe^{2+}		$Fe^{2+}/\Sigma Fe$
			IS, mm/sec	QS, mm/sec	IS, mm/sec	QS, mm/sec	
Di + 1% Fs*	1425	air	...	...	1.014	1.918	0.82
Di + 2.5% Fs	1425	air	0.524	1.073	0.998	2.011	0.60
Di + 5% Fs	1425	air	0.479	1.027	0.982	2.032	0.58
Di + 10% Fs	1425	air	0.372	1.114	0.921	2.214	0.36
DW50 + 5% Fs	1525	air	0.449	1.028	0.980	2.057	0.55
DW50 + 5% Fs	1525	O_2	0.453	1.064	0.956	2.071	0.47
Di + 5% Fs	1525	air	0.492	1.060	0.984	2.048	0.61
DE50 + 5% Fs	1525	air	0.532	1.053	0.987	2.003	0.64
DE50 + 5% Fs	1525	O_2	0.473	1.026	0.977	2.035	0.60
WO + 5% Fs	1585	air	0.422	0.965	0.961	2.044	0.51
WO + 10% Fs	1585	air	0.382	0.939	1.048	1.904	0.35
DW50 + 5% Fs	1585	air	0.500	1.002	0.999	2.002	0.60
Di + 5% Fs	1585	air	0.484	1.024	1.024	2.046	0.60
DE50 + 5% Fs	1585	air	0.510	1.001	1.051	2.034	0.867
En + 5% Fs*	1585	air	...	...	0.923	1.835	0.78

**Two-line fit.*

IS, isomer shift relative to Fe metal; QS, quadrupole splitting; Di, $CaMgSi_2O_6$; DW50, 50 mole % $CaMgSi_2O_6$–50 mole % $Ca_2Si_2O_6$; DE50, 50 mole % $CaMgSi_2O_6$–50 mole % $Mg_2Si_2O_6$; En, $MgSiO_3$; Fs, $FeSiO_3$ (added as a component with Fe_2O_3 in the starting material).

spectra of quenched melts on various metal oxide–silica joins as a function of metal oxide/silica ratio and type of metal oxide must be considered. A considerable amount of data is already available (Brawer and White, 1975, 1977; Furukawa *et al.*, 1978; Verweij, 1979a,b; Virgo *et al.*, 1980; Mysen *et al.*, 1980; Virgo and Mysen, in preparation). The data base provided by these authors includes NBO/Si (nonbridging oxygen per silicon) from near 4 (orthosilicate) to 0 (three-dimensional network), and cations such as K^+, Na^+, Li^+, Ca^{2+}, Mg^{2+}, and Pb^{2+}. In summarizing these data, Brawer and White (1977) and Virgo *et al.* (1980) concluded that the Raman spectra of melts with given metal oxide/silica ratio do not depend on the type of metal cation. They inferred from this conclusion that the anionic structure of binary metal oxide–silicate melts does not depend on the type of metal cation.

The most accurate spectroscopic information on the structure of such binary melts can be obtained

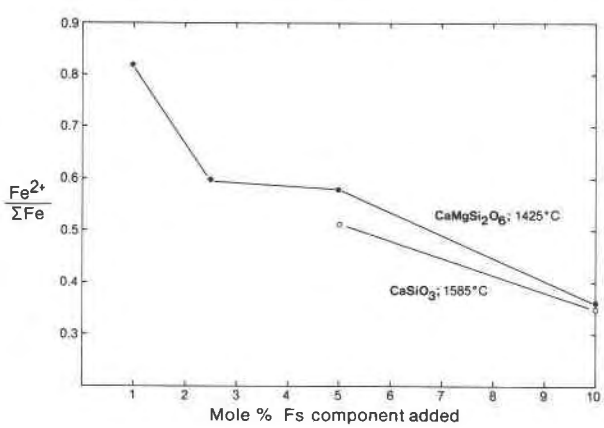

Fig. 7. $Fe^{2+}/\Sigma Fe$ of quenched melts on the join $CaSiO_3$–$MgSiO_3$–$FeSiO_3$ as a function of Fs content.

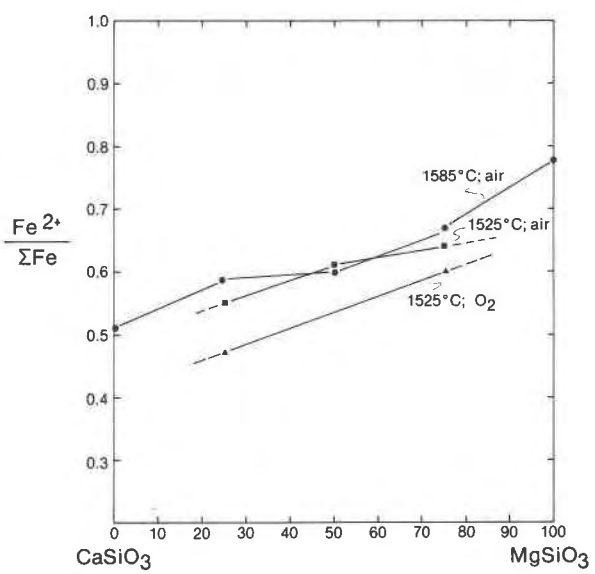

Fig. 8. $Fe^{2+}/\Sigma Fe$ of quenched melts on the join $CaSiO_3$–$MgSiO_3$ with 5 mole percent Fs component added.

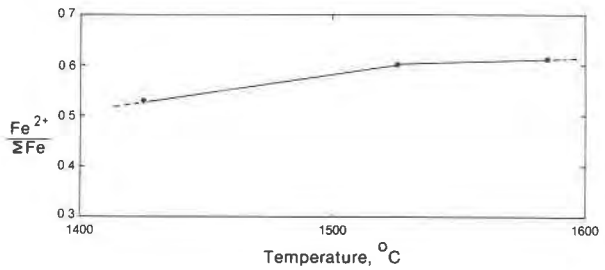

Fig. 9. $Fe^{2+}/\Sigma Fe$ of quenched melt of $CaMgSi_2O_6$ + 5 mole percent $FeSiO_3$ component as a function of temperature in air.

from alkaline-earth silicate melts, as such melts are not significantly hygroscopic and do not suffer potential metal-cation volatilization during preparation (Kracek, 1930). Among the joins of alkaline-earth silicates, the join with the widest range of M/Si is $CaO–MgO–SiO_2$ (Ca/Mg = 1) (Virgo *et al.*, 1980; Mysen *et al.*, 1980). Eight spectra from melts on that join are reproduced in Figure 10 (see also Table 5). Compositionally, these melts differ only in (Ca + Mg)/Si, as indicated in Figure 10.

The dominant feature of each spectrum is the intense, slightly asymmetric band in the region between 600 and 670 cm^{-1} combined with an intense, high-frequency envelope in the region between 800 and 1100 cm^{-1}. All these bands are strongly polarized. All the bands, with the exception of that in the region 600–670 cm^{-1}, remain at the same frequency as M/Si varies (Fig. 10). The latter bands shift to higher frequency as a systematic function of increasing M/Si.

In melts with M/Si between 1.9 (DM 95) and 1.18 (DM 25), there is a very strong sharp band near 870 cm^{-1} and a less intense band near 900 cm^{-1}. The 870 cm^{-1} band remains in all spectra of melt compositions from DM 95 to SD 40. The 900 cm^{-1} band disappears somewhere between DM 25 and Di composition (M/Si = 1.18 and 1.0, respectively). It appears that the intensity of the 900 cm^{-1} band passes through a maximum for melt compositions near DM 58. The intensity of the 870 cm^{-1} decreases as a continuous function of decreasing M/Si. Both bands remain polarized in the entire compositional range.

The 870 cm^{-1} band is by far the most intense band in crystalline orthosilicates (Furukawa *et al.*, 1978; Verweij and Konijnendijk, 1976). Furukawa *et al.* (1978), Verweij and Konijnendijk (1976), Verweij (1979a,b) and Furukawa and White (1980) assigned this band to symmetric stretch vibrations of nonbridging oxygen bonds in separate SiO_4^{4-} tetrahedra (symbol: $Si–O^{2-}$). This assignment is retained here.

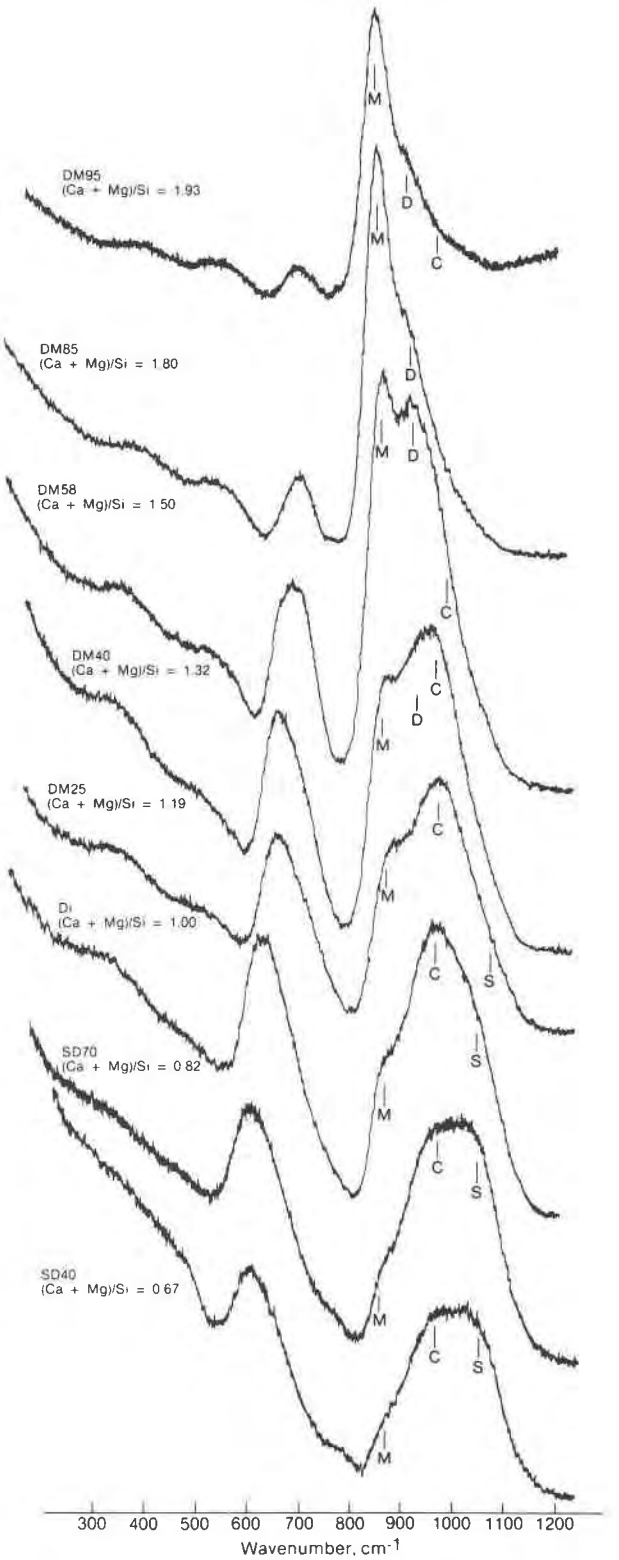

Fig. 10. Raman spectra of quenched melts on the join $CaO–MgO–SiO_2$ (Ca/Mg = 1) at 1 atm and 1650°C. M, D, C, S: band positions of symmetric stretch bands derived from vibrations in structural units with NBO/Si = 4, 3, 2, and 1, respectively.

Table 5. Raman data of quenched melts on the join CaO–MgO–SiO_2 (Ca/Mg = 1) at 1 atm and 1650°C

Composition	Wavenumber, cm^{-1}							
DM95	380w,p(bd)	530m,p(bd)	700w,p	–	848s,p	903m,p	977mw,p	–
DM85	380w,p(bd)	527m,p(bd)	700w,p	–	847s,p	903m,p	978m, p	–
DM58	343w,p(bd)	513m,p(bd)	686w,p	–	860s,p	910s,p	973m,p	–
DM40	340w,p(bd)	500m,p(bd)	660m,p	–	863s,p	908m,p	973m,p	–
DM25	340w,p(bd)	–	655m,p	–	860s,p	913w,p	973s,p	–
DI	340w,p(bd)	–	630m,p	770vw(sh)	867m,p	–	967s,p	1060m,p
SD70	–	–	622s,p	770,w	873w,p	–	959s,p	1063m,p
SD40	–	500vw,(sh)	610s,p	–	873vw	–	955s,p	1063m,p

Symbols: vw - very weak, w - weak, mw - medium to weak, m - medium, ms - medium to strong, s - strong
p - polarized, (bd) - broad, (sh) - shoulder.
Uncertainties: Strong to weak bands - ± 5 cm^{-1}. Very weak bands - ∿ 10 cm^{-1}. Shoulders - ± 15-20 cm^{-1}
Compositions are defined in Fig. 10.

The 900 cm^{-1} band is the major band in crystalline pyrosilicates (Lazarev, 1972; Sharma and Yoder, 1979). Since its frequency is higher than that of the symmetric $Si–O^{2-}$ stretch band (870 cm^{-1}), it is polarized, and its frequency coincides with the main band in crystalline pyrosilicates, this band is interpreted as due to the presence of dimer structural units in the melt ($Si_2O_7^{6-}$). Its frequency is independent of the melt composition. We conclude, therefore, that the NBO/Si of this structural unit does not change with changing composition of the melt. Further support for this interpretation is found in the observation that the maximum intensity of the 900 cm^{-1} band is found in melts with a stoichiometry close to that of a dimer (NBO/Si = 3).

The high-frequency envelope (Fig. 10) also contains a band near 970 cm^{-1} (found in all compositions on this join) and one near 1070 cm^{-1} (found in melt compositions with M/Si equal to or less than that of metasilicate). Both bands are polarized. The intensity of the 970 cm^{-1} band increases relative to the other bands in the high-frequency envelope in the compositional range between DM 95–Di and decreases as the M/Si is decreased further. The intensity of the 1070 cm^{-1} band increases as a function of decreasing M/Si at M/Si<1. The frequencies of both bands are independent of M/Si. Note that the frequency of the band between 600 and 670 cm^{-1} decreases from about 650 cm^{-1} in metasilicate melt (M/Si = 1) to near 600 in SD 40 melt (M/Si = 0.67).

On the basis of frequencies, polarization characteristics, and analogy with crystalline meta- and disilicates (Etchepare, 1972; Furukawa and White, 1980), we conclude that the 970 cm^{-1} band is a symmetric $^-O–Si–O^-$ stretch band and the 1070 band is a symmetric $^-O–Si–O^0$ stretch band. The associated deformation bands are those at 650 and 600 cm^{-1}, respectively. This conclusion accords with that of Verweij (1979a,b) and Furukawa and White (1980). The $^-O–Si–O^-$ stretch vibration may be derived from structural units with NBO/Si = 2 (*e.g.*, chain) and the $^-O–Si–O^0$ from structural units with NBO/Si = 1 (*e.g.*, sheet). The exact structural assignments will be discussed below.

The most important observation made from the above assignments of the Raman spectra is that there appears to be a unique set of coexisting anionic structural units in specific ranges of NBO/Si of the melts. The proportions of the individual structural units vary as a function of bulk NBO/Si (M/Si), but the NBO/Si of each unit does not. In Table 6, the anionic units are defined on the basis of the average NBO/Si, using the data summarized above in conjunction with the published data summarized by Virgo *et al.* (1980) and Mysen *et al.* (1980). Several aspects of these conclusions warrant further comment. In comparison to some models of melt structure (*e.g.*, Masson, 1977), the model is strikingly simple. This simplicity should not be surprising, since when comparing with crystal structures of silicates only a few anionic structures can be found (see Dent Glasser, 1979, for review). The same structural units have been found in silicate melts. In silicate crystal chemistry, the metal cations are considered important in controlling the type of polymers that will occur. Polymer theory as applied to silicates (*e.g.*, Masson, 1977) does not take the metal cations into account.

Table 6. Raman frequencies of the stretch vibrations of specific Si-rich anionic structural units in silicate melts (after Virgo *et al.*, 1980)

Structural unit	NBO/Si	Frequency (cm^{-1})	Characteristics of vibrational mode
SiO_4^{4-}	4	850–880	Symmetric stretch
$Si_2O_7^{6-}$	3	900–920	Symmetric stretch
$Si_2O_6^{4-}$	2	950–980	Symmetric stretch
$Si_2O_5^{2-}$	1	1050–1100	Symmetric stretch
SiO_2	0	1060,1190	antisymmetric stretch

Previous models of melt structure include features such as trimers, tetramers, pentamers, *etc.*, in addition to rings and branched chains. The experimental basis for most of these models is from organic chemistry. As applied to silicates, the experimental basis has been chromatographic data derived from trimethylsilyl derivatives of the silicates (TMS-derivatives). Limitations and inconsistencies of such data have been discussed elsewhere (*e.g.*, Masson, 1977; Kuroda and Kato, 1979) and are not pursued here. It is merely concluded that structural data of silicate melts derived from TMS-derivatives are not reliable.

Polymer theory predicts that there is a positive correlation between the number of silicons in the polymers and the proportion of various types of polymers and the NBO/Si of the melt. In Raman spectroscopic studies, such a correlation would result in a successive increase of the frequency of Si–O stretch bands as a function of decreasing NBO/Si (M/Si) (*e.g.*, Lazarev, 1972; Brawer and White, 1975; Furukawa and White, 1980; see also Table 6). On this basis it would be expected that if anionic structural units with degree of polymerization between chains and dimers were formed in the melts in the various binary metal oxide–silicate joins, new bands would occur between 900 and 970 cm^{-1} or bands such as that at 900 cm^{-1} would shift to higher frequency as a function of decreasing M/Si of the melt. No such spectroscopic evidence is present in our data, nor in any related published data (Brawer and White, 1975, 1977; Furukawa *et al.*, 1978; Verweij, 1979a,b; Verweij and Konijnendijk, 1976; Furukawa and White, 1980; Mysen *et al.*, 1980). We conclude, therefore, that structural units with NBO/Si between that of a dimer and that of a chain (3 and 2, respectively) do not exist in significant amounts in silicate melts.

The structural units with NBO/Si = 2 have been referred to as a chain. Simple rings have, however, the same NBO/Si. The idea of ring structures in silicate melts has experimental support in the TMS-derivative work (as summarized by Masson, 1977). Ring structures have also been suggested in melts on binary metal oxide–silicate joins on the basis of the viscous behavior of such melts (*e.g.*, MacKenzie, 1960; Bockris and Reddy, 1970). Spectroscopic evidence relevant to ring structures is scarce. Lazarev (1972) discussed spectroscopic imprints of ring structures with up to 6 silicons. In the simple $Si_3O_9^{6-}$ ring, there is a strong silicon–oxygen deformation band near 750 cm^{-1}. No such band exists in the data in Figure 10 and other relevant data discussed elsewhere, and therefore this type of ring probably does not occur. Larger ring structures show stretch bands slightly above 1100 cm^{-1}. On a spectroscopic basis alone it is not likely, but not impossible, that the 1070 cm^{-1} band could, in fact, be such a band (*e.g.*, S-band in Fig. 10). Mass-balance considerations require, however, that in metasilicate melts, for example, the existence of structural units with NBO/Si = 4 and 2 also requires the existence of structural units with NBO/Si < 2. Careful analysis by, in particular, Verweij (1979a,b) and Furukawa and White (1980) resulted in the conclusion that the band between 1070 and 1100 in their melts (Na_2O–SiO_2 join) was due to a band with NBO/Si = 1. Inasmuch as this band also exists in alkaline-earth metasilicates, it is attractive to assign this band to that structural unit. One might suggest, however, that the ^-O–Si–O^0 vibrational mode stems from end units in a linear structure. Such an interpretation does not provide for structural units in the melt that would satisfy the mass-balance requirements, and neither would the ring-structure assignment. It might also be suggested that the presence of branched chains or multiple chains could constitute the structural unit(s) with NBO/Si < 2. The end result of such branching is, of course, a sheet. Intuitively, it would be expected that branching would be continuously increasing as the M/Si of the melt decreased. If the S-band in Figure 11 were such a band, for example, one would expect its frequency to increase. It does not. Furthermore, according to survey of silicate mineral structures (Dent Glasser, 1979), branched chains do not exist, presumably for energetical reasons. There is no reason, therefore, why one would expect such structures in a melt. Instead, chains and sheets are formed.

An option that does exist to explain the 1070 cm^{-1} band is multiple chains (finite sheet). It cannot be established from the Raman data whether the S-band (Fig. 10) is due to such a finite sheet or due to an infinite sheet. The simplest interpretation is an infinite

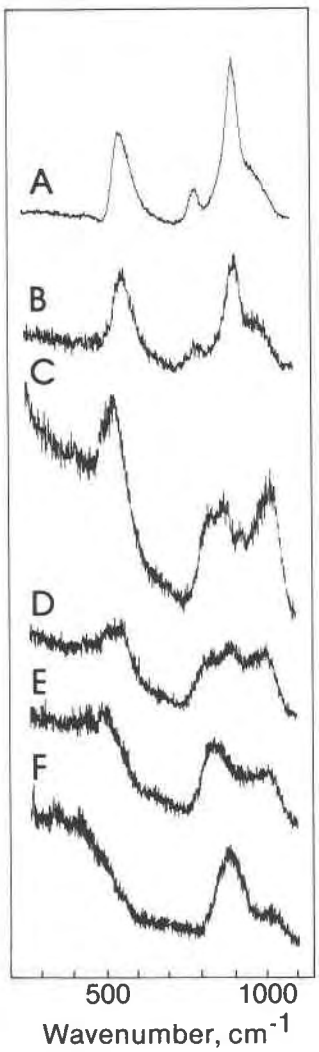

Fig. 11. Unpolarized Raman spectra of quenched melts on the join Na_2SiO_3–$NaFe^{3+}Si_2O_6$ in air at 1400°C. (A) NS. (B) NS94Ac6. (C) NS85Ac15. (D) NS75Ac25. (E) NS50Ac50. (F) Ac100. (Kr^+ ion laser with 200–400 mW power.)

sheet (NBO/Si = 1) and this interpretation is adhered to here. This conclusion is not absolutely certain, however.

Iron was added to metasilicate melts of Na^+(NS), Ca^{2+} (Wo), $(Ca,Mg)^{2+}$ (Di) and Mg^{2+} (En). The Raman spectra of these melts will be discussed first (Fig. 11A, 12; see also Tables 7 and 8). The high-frequency envelopes of these spectra were deconvoluted into individual bands (Fig. 13), in order to get an impression of the relative intensities of the bands in the high-frequency envelopes. In the deconvolution procedure, we assumed that the bands were Gaussian, were symmetric, and that the background was horizontal. The Gaussian line-shape was derived from selected portions of the high- and low- frequency limbs of the high-frequency envelopes. Extrapolation of the Rayleigh tail from frequencies less than 500 cm^{-1}, using exponential functions, to the spectral region of the high-frequency envelope indicates that the assumption of horizontal background is appropriate. Finally, bands were only fitted when indicated by the form of the raw Raman, high-frequency envelope.

With the exception of the broad, weak band near 350 cm^{-1} in quenched Wo melt (Fig. 12), the same Raman bands are found in all four metasilicate melts. The spectra consist of a strong, somewhat asymmetric band in the region between 620 and 650 cm^{-1}, a distinct band or shoulder near 870 cm^{-1}, a strong band near 970 cm^{-1} and a shoulder between 1050 and 1100 cm^{-1}. These bands are polarized. All the bands were discussed under Figure 10 (see also Tables 5 and 6), and no further discussion is necessary. The additional band near 350 cm^{-1} in quenched Wo melt was also noted by Brawer and White (1977)

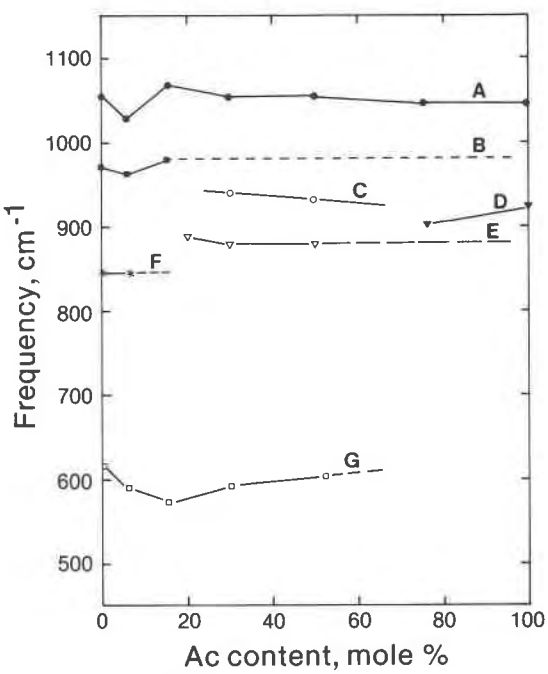

Fig. 12. Frequency shift of unpolarized Raman bands as a function of Ac content [(Fe)Si]O^0 on the join Na_2SiO_3–$NaFeSi_2O_6$ at 1400°C in air. (A) (Si, Fe)–O^0 stretch mode. (B) (Si, Fe)–O^- stretch mode; dashed line denotes inferred extension (see discussion in text). (C) Mixed (Fe,Si)–O^- and (Fe,Si)–O^0 stretch modes (see discussion in text). (D) Mixed (Fe, Si)–O^0 and (Fe,Si)–O^- stretch modes (see discussion in text). (E) (Fe,Si)–O^- stretch mode; dashed line denotes inferred extension (see discussion in text). (F) Si–O^{2-} stretch mode. (G) (Si,Fe)–O^0 rocking mode.

Table 7. Vibrational frequencies and band assignments of quenched melts on the join Na_2SiO_3–$NaFe^{3+}Si_2O_6$ at 1400°C in air

Composition	Wavenumber, cm^{-1}							
NS	...	...	619,s,p	847,w,p	...	...	970,s,p	1070,m(sh),p
NS94Ac6	...	...	591,s,p	847,w,p	...	...	962,s,p	1032,m(sh),p
NS85Ac15	...	...	577,s,p	...	887,m,p	928,m,p	978,m,p	1065,m,p
NS75Ac25	...	551,m,p	590,s,p	...	877,m,p	...	940,m,p	1052,m,p
NS50Ac50	480,w,p	540,s,p	605(sh),p	...	882,m,p	...	931,m,p	1053,s,p
NS25Ac75	477,s,p	540,m(sh),p	...	...	...	897,m,p	...	1047,m,p
Ac100	451,s,p	541,m(sh),p	...	...	...	925,s,p	...	1047,m,p

Symbols: w, weak; m, medium; s, strong; (sh), shoulder; p, polarized.
The uncertainty is 10 cm^{-1} for weak bands, 5-6 cm^{-1} for medium bands and 3-4 cm^{-1} for strong bands. For shoulder add 100% to uncertainty.

and is probably due to vibrations within Ca–O polyhedra.

The Raman data for metasilicate melts indicate, therefore, that the anionic structural units are SiO_4^{4-} (NBO/Si = 4), $Si_2O_6^{4-}$ (NBO/Si = 2), and $Si_2O_5^{2-}$ (NBO/Si = 1). Our interpretation suggests, therefore, that in metasilicate melts the chain units are partially disproportionated into monomers (SiO_4^{4-}) and sheets ($Si_2O_5^{2-}$):

$$3Si_2O_6^{4-} \rightleftharpoons 2SiO_4^{4-} + 2Si_2O_5^{2-} \qquad (1)$$

Raman spectroscopic measurements have been carried out on quenched melts on the join Na_2SiO_3–$NaFe^{3+}Si_2O_6$ (NS–Ac) (Table 7) where the Mössbauer data indicated that within the detection limit of the Mössbauer technique all iron was present in the ferric state. No spectra could be taken on samples with ferrous iron because of oxidation of Fe^{2+} to Fe^{3+} due to surface heating by the laser, photo-oxidation, or both. Consequently, Raman data for iron-bearing alkaline-earth metasilicate melts could not be acquired.

The Raman spectrum of acmite melt formed in air and quenched from 1400°C is shown in Figure 11 and band assignments are shown in Table 7. The spectrum consists of four bands. The strongest band is at 925 cm^{-1} and a weaker one is at 1047 cm^{-1}. In addition, there is a shoulder near 540 cm^{-1} and another one near 450 cm^{-1}.

The results of Mössbauer (Table 1), EXAFS, and radial distribution analysis (Brown *et al.*, 1978) have shown that Fe^{3+} is in tetrahedral coordination in melts of $NaFe^{3+}Si_2O_6$ composition when quenched in air. This conclusion implies that in the absence of Fe^{2+} quenched Ac melt has a three-dimensional network structure. In compositions analogous to those on the joins $NaAlO_2$–SiO_2, $CaAl_2O_4$–SiO_2, $NaFeO_2$–SiO_2, and $NaGaO_2$–SiO_2 (Virgo *et al.*, 1979), it was shown that at least two high-frequency (Si,Al)–O^0, (Si,Fe)–O^0, and (Si,Ga)–O^0 stretch bands occur. Their frequencies and intensities shift systematically with Si/(Si + T), where T = Al, Fe, or Ga. In light of these observations, we suggest that the two high-frequency bands in quenched Ac melt are due to antisymmetric (Si,Fe)–O^0 and (Fe,Si)–O^0 stretching.[2]

In addition to the two characteristic high-frequency bands, a distinct shoulder occurs near 450 cm^{-1}. This shoulder is probably an (Si,Fe)–O^0 rocking mode. The band characteristically occurs in the spectral region between 450 and 500 cm^{-1} in all three-dimensional melts in the system Na_2O–CaO–Ga_2O_3–Al_2O_3–SiO_2 (Bates *et al.*, 1974; Virgo *et al.*, 1979).

The Raman spectra of quenched melts of compositions on the join Na_2SiO_3–$NaFe^{3+}Si_2O_6$ are also shown in Figure 11, and the band assignments are given in Table 7. The frequency shifts of the important bands as a function of bulk composition of the quenched melt are shown in Figure 14.

Mixing of Na_2SiO_3 and $NaFe^{3+}Si_2O_6$ components constitutes combining a three-dimensional network unit with characteristic bands at 1047, 925, 540, and 451 cm^{-1} and a less polymerized melt that consists of

Table 8. Vibrational frequencies and band assignments of melts on the join $CaSiO_3$–$MgSiO_3$

Composition	Wavenumber, cm^{-1}			
$CaSiO_3$	637,s,p	979,s,p	981,s,p	1070,s(sh),p
$CaMgSi_2O_6$	640,s,p	877,m(sh),p	980,s,p	1070,s(sh),p
$MgSiO_3$	640,s,p	882,m(sh),p	975,s,p	1058,m(sh),p

Symbols and uncertainty as in Table 5.

[2] The notations (Si,Fe)–O^0 and (Fe,Si)–O^0, respectively, imply Si-rich and Fe-rich (Si,Fe)–O–(Si,Fe) stretch vibrations. The analogous rotations for nonbridging oxygen bands are (Si,Fe)–O^- and (Fe,Si)–O^-.

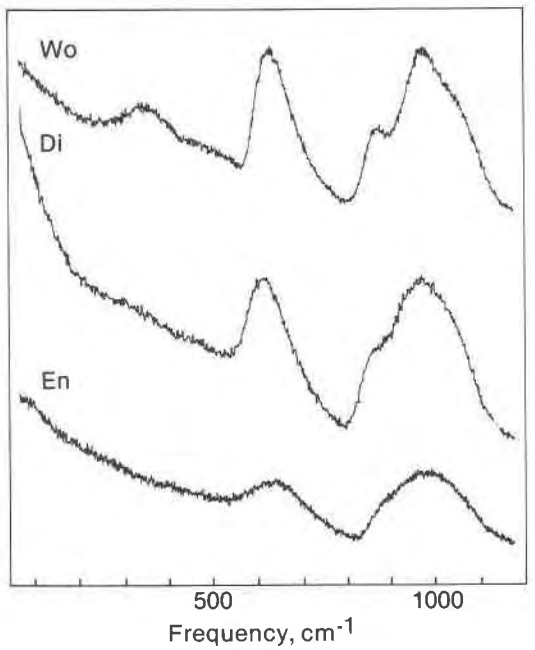

Fig. 13. Unpolarized Raman spectra of quenched (1585°C) melts on the join $CaSiO_3$–$MgSiO_3$. Wo, $CaSiO_3$; Di, $CaMgSi_2O_6$; En, $MgSiO_3$. (Al^+ ion laser with 200–400 mW power.)

monomer, chain, and sheet units with characteristic bands at 1070, 970, 850, and 618 cm^{-1} (Fig. 11, Table 7). Addition of 25 mole percent NS component to Ac results in resolved bands at 1047, 897, 540, and 477 cm^{-1}. The band at 897 cm^{-1} is asymmetric and much broader than the 925 cm^{-1} band in quenched Ac melt. The asymmetry of this band may indicate that it, in fact, consists of two unresolved bands. One band may be the 925 cm^{-1} band of quenched Ac melt [(Fe,Si)–O^0 stretch]. The other band is new and occurs at a wave number between 800 and 900 cm^{-1}. If this interpretation of the asymmetric 897 cm^{-1} band is correct, this latter band may be due to nonbridging oxygen in the melt and could be either an ^-O–(Fe,Si)–O^0 or an ^-O–(Fe,Si)–O^- stretch vibration. The 1047 cm^{-1} band in NS25Ac75 is more intense relative to the rest of the high-frequency envelope than in quenched Ac melt. Inasmuch as the proportion of Ac component is decreased in NS25Ac75 melt relative to that of pure Ac composition, probably the 1047 cm^{-1} band in quenched NS25Ac75 melt either reflects a new vibrational mode or is a combination of two modes. In the latter case, one mode may be the (Si,Fe)–O^0 stretch vibration of Ac melt and the other vibration may reflect a nonbridging oxygen. We suggest that the increased intensity of the 1047 cm^{-1} band is due to ^-O–(Si,Fe)–O^0 stretching. Its frequency is lower than that for pure NS quenched melt (Fig. 14) because of (Si,Fe) coupling. As a result of this band assignment, it must be concluded that the unresolved low-frequency component of the 894 cm^{-1} band is a highly coupled ^-O–(Fe,Si)–O^- stretch vibration. In conclusion, quenched melt of NS25Ac75 composition consists of a combination of structural units with NBO/T (where T = Si + Fe) = 0, 1, and 2.

In quenched NS50Ac50 melt, the two low-frequency bands suggested for NS25Ac75 melt (as a result of the asymmetric 897 cm^{-1} band) are partially resolved (Fig. 11). One band is found at 882 cm^{-1} and the other near 930 cm^{-1}. In this melt composition, the 1047 cm^{-1} band is shifted to 1053 cm^{-1}, and its intensity relative to the rest of the high-frequency envelope has increased further compared with that of quenched NS25Ac75 melt. The intensity increase is a result of more sheet units in the more NS-rich quenched melt. The location of the 882 cm^{-1} band in the spectrum is probably still somewhat influenced by the weakened (Fe,Si)–O^0 stretch vibration at 925 cm^{-1}. The shoulder on this band also indicates the presence of a second band near 930 cm^{-1}. This band

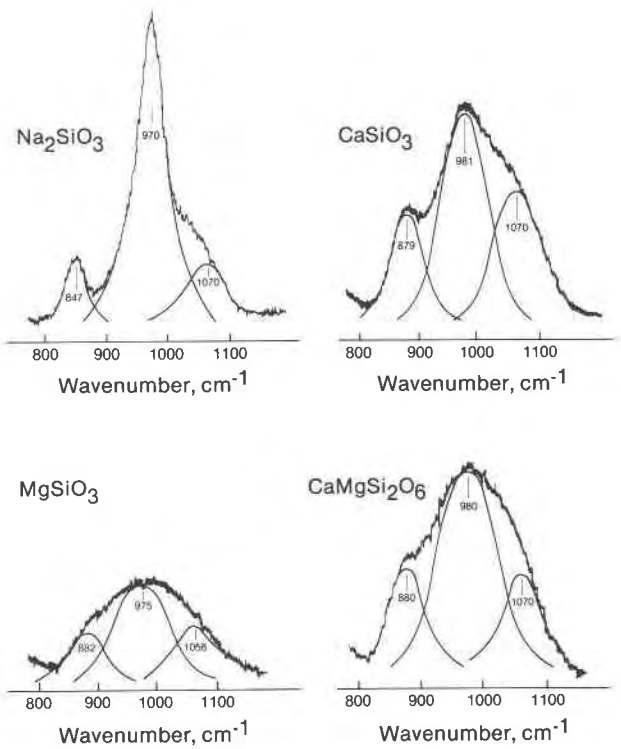

Fig. 14. High-frequency envelope of Raman spectra of quenched metasilicate melts with Gaussian curves fitted inside the envelope to match positions and total area of high-frequency envelope.

could be the (Fe,Si)–O^0 stretch vibration with a slightly lowered Fe content. Alternatively, it could be another band that has appeared. If the latter suggestion is correct the frequency of this band might shift to a higher wave number as the NS content of the quenched melt is increased, as indicated by the data in Figure 14. This feature will be discussed below. A shoulder occurs near 600 cm^{-1} in quenched melt of NS50Ac50 composition. Its frequency is near the 620 cm^{-1} band, corresponding to the deformation mode of pure metasilicate melt (Figs. 11 and 12), and may be due to a similar vibration. In conclusion, quenched melt of NS50Ac50 composition consists of the same structural units as quenched NS25Ac75 melt (3D: NBO/T = 0, sheet: NBO/T = 1 and chain: NBO/T = 2). The chain and sheet units are more pronounced and the 3D unit less pronounced in this melt than in quenched melt of NS25Ac75 composition, as would also be expected because of the higher NS content of this quenched melt.

The high-frequency envelope of quenched NS75Ac25 melt shows the same bands as quenched NS50Ac50 melt except that their frequencies and intensities are slightly different (Figs. 11 and 14). The highest frequency band (1052 cm^{-1}) is at the same position as in quenched NS50Ac50 melt, but it has become more intense (Fig. 11). The 931 cm^{-1} band in quenched NS50Ac50 melt has shifted to 940 cm^{-1} and is now clearly resolved. We suggest that this band is a combination of the 925 cm^{-1} band of (Fe,Si)–O^0 stretching and a new band at higher frequency, which probably is the 970 cm^{-1} band found in pure NS melt, a band assigned to ^-O–Si–O^- stretching. The higher frequency of this band compared with the ^-O–(Fe,Si)–O^- stretch band below 900 cm^{-1} indicates much less extensive (Fe,Si) coupling. With the exception of this conclusion, the band assignments of the high-frequency envelope of the Raman spectrum of quenched NS75Ac25 melt are the same as for quenched NS50Ac50 melt. The greater intensities of the bands assigned to depolymerized units are due to the greater proportion of NS component in this quenched melt. In fact, except for the above discussion concerning the 925 cm^{-1} band, no clear evidence exists for the presence of a 3D unit in quenched melt of NS75Ac25 composition.

In quenched melt of NS85Ac15 composition the band at 940 cm^{-1} in NS75Ac25 occurs at 978 cm^{-1} and is clearly resolved. We conclude, therefore, that the band that first occurs at 931 cm^{-1} in NS50Ac50 composition now is at 978 cm^{-1}. It is not clear whether this evolution is a result of diminished interference from the 925 cm^{-1} band as the Ac content decreases and increased intensity as the NS content increases, or a result of diminished (Si,Fe) coupling of this vibration as the Fe content of the quenched melts decreases. Note, however, that the other band assigned to ^-O–(Si,Fe)–O^- stretch vibration (880 cm^{-1}) does not change its frequency significantly as a function of Ac content of the melt; only its intensity decreases. We suggest that the same behavior takes place for the 970 cm^{-1} band. Its frequency remains constant as the bulk composition changes, but the intensity increases at the expense of the more (Si,Fe)-coupled vibrations.

The diminished influence of Fe on the band frequencies of quenched NS85Ac15 melt is also indicated by the increased frequency of the 1050 cm^{-1} band, now found at 1065 cm^{-1}. The 1065 cm^{-1} frequency is nearly the same as for pure NS melt (Fig. 11, Table 7). This band is probably due to ^-O–Si–O^0 stretching with insignificant (Si,Fe) coupling.

The spectrum of quenched NS94Ac6 melt closely resembles that of quenched melt of NS100 composition (Fig. 11) and differs substantially from the spectra of more Fe-rich compositions. The same bands are observed in the spectra of quenched NS100 and NS94Ac6 melts, although there are systematic frequency shifts (Fig. 14). The 1070 cm^{-1} band in pure NS occurs at 1032 cm^{-1}, and the strong band at 970 cm^{-1} is found at 962 cm^{-1}. The weak band at 847 cm^{-1} in quenched NS melt is at 847 cm^{-1} in NS94Ac6 melt as well. The 619 cm^{-1} band in pure NS melt is at slightly lower frequency in NS94Ac6 melt, probably reflecting a slightly higher degree of polymerization (Brawer, 1975). The 1032 cm^{-1} band in quenched NS94Ac6 melt is assigned to ^-O–(Si,Fe)–O^0 stretching (sheet), and the 962 cm^{-1} band to ^-O–(Si,Fe)–O^- stretching (chain). The 847 cm^{-1} band reflects the presence of isolated SiO_4^{4-} tetrahedra in the quenched melt. There is no evidence for additional Raman bands that may be ascribed to isolated $NaFeO_4^{4-}$ tetrahedra. The intensity of the 1032 cm^{-1} band relative to that at 962 cm^{-1} is greater than the intensity ratio of the analogous bands in pure quenched NS melt. We conclude, therefore, that even though monomers, chains, and sheets are present in both quenched melts, the proportion of sheet units is greater in NS94Ac6 quenched melt than in NS melt.

In summary, mixing of Na_2SiO_3 (NS) and $NaFe^{3+}Si_2O_6$ (Ac) components results in a melt that to a first approximation resembles mixing of SiO_2 and Na_2SiO_3 when the NS melt becomes more po-

lymerized as the Ac content of the melt is increased. Ferric iron is distributed among all structural units in the melts, with the possible exception of isolated tetrahedra. The latter structural unit has a limited stability field, however, as it is not observed in melts with more than 15 mole % Ac component.

The spectra are also interpreted to indicate that the stretch vibrations of the various structural units occur in pairs—one indicates greater Si(Fe)-coupling than the other. This observation may indicate that both Fe-rich and Si-rich structural units occur in these melts.

The anionic structures of these melts differ in the extent of disproportionation, which can be expressed with the intensity ratios $I(970)/I(870)$ and $I(970)/I(1070)$ (Table 9). The larger the extent of disproportionation, the smaller the intensity ratios. Tables 9 and 10 show that the extent of disproportionation of metasilicate melts increases in the order NS < En < Di < Wo.

Redox equilibria

Despite the similarity of the anionic silicate units in metasilicate melts, ferric iron enters tetrahedral coordination only in the presence of Na^+. Metasilicate melts of the alkaline earths have ferric iron in octahedral coordination. In all other alkali silicate melts investigated so far (Mysen and Virgo, 1978; Brown *et al.*, 1978: Seifert *et al.*, 1979b), ferric iron enters tetrahedral coordination, probably as an $NaFeO_2$ complex, in analogy with the $NaAlO_2$ complex found in Al-bearing melts (Virgo *et al.*, 1979; Brawer and White, 1977). It may be inferred, therefore, that in alkali-bearing melts, Fe^{3+} and Al^{3+} often play similar structural roles.

Solution of Ac component in NS melt in air (no detectable ferrous iron) results in the formation of structural units with $NBO/Fe^{3+} = 1$ and 2 ($Fe_2O_5^{4-}$ and $Fe_2O_6^{6-}$, respectively), in addition to the structural units expressed with equation 1. As $f(O_2)$ is lowered below that of air, ferrous iron is formed in these melts. Our data and published information (Mao *et al.*, 1973; Bell and Mao, 1974; Boon and Fyfe, 1972; Mysen and Virgo, 1978) indicate that Fe^{2+} is a network modifier. The redox equilibrium involving ferric iron in tetrahedral coordination and ferrous iron in octahedral coordination may be expressed with the equation:

$$4Fe(IV)O_2^- + 3O^-(NBO) \rightleftarrows 4Fe(VI)O_6^{10-} + O_2 \quad (2)$$

The nonbridging oxygen (NBO) required to form the octahedral ferrous ion complex, FeO_6^{10-}, may be derived from the anionic silicate structural units. Equation 1 may be combined with equation 2, therefore, in order to describe the interaction between redox equilibria of iron and the anionic structure of silicate melts:

$$72Si_2O_6^{4-} + 4Fe(IV)O_2^- \rightleftarrows 54Si_2O_5^{2-} + 36SiO_4^{4-} + 4Fe(VI)O_6^{10-} + O_2 \quad (3)$$

The $Fe^{3+}/\Sigma Fe$ of such melts depends, therefore, not only on $f(O_2)$, but also on the NBO/T of the melt, a conclusion also made by Lauer (1977) and Lauer and Morris (1977).

We concluded above, on the basis of the isomer shifts of ferric iron, that Fe^{3+} will not be a network former in melts where there is only alkaline-earth metal network modifier for local charge balance. The redox equilibria of network modifiers in such melts do, however, also depend on the anionic structure of the silicate melts, as also shown by Lauer and Morris (1977). Those authors concluded, for example, that the redox equilibrium for a network-modifying cation shifts to a more reduced state as the size of the network-modifying cations in the melt decreases. This conclusion accords with our observation for iron oxides in melts on the join $MgSiO_3$–$CaSiO_3$ (Fig. 8), where the $Fe^{3+}/\Sigma Fe$ decreases as Ca/(Ca + Mg) decreases. Lauer and Morris (1977) expressed such relationships with a Φ-function that could be determined experimentally without further consideration for the structure of the silicate melts. We may discuss this dependence in terms of the disproportionation of anionic polymers such as shown in equation 1. According to the results summarized in Table 8, equation 1 shifts to the left as Ca/(Ca + Mg) of the melt

Table 9. Intensity ratios $I(970)/I(870)$ and $I(970)/I(1070)$, in quenched silicate melts

Composition	$I(970)/I(870)$	$I(970)/I(1070)$
$MgSiO_3$	3.95	3.53
$CaSiO_3$	2.69	1.77
$CaMgSi_2O_6$	3.57	2.53
Na_2SiO_3	8.17	5.15

Table 10. Percentage change of $I(970)/I(870)$ and $I(970)/I(1070)$ of quenched melts on the join $CaSiO_3$–$MgSiO_3$ relative to quenched melt of Na_2SiO_3 composition

Composition	$I(970)/I(870)$	$I(970)/I(1070)$
$CaSiO_3$	-67	-65
$CaMgSi_2O_6$	-56	-51
$MgSiO_3$	-52	-31

decreases. Whether this is because both the monomer and the sheet unit are affected by the decreasing size of the cation or only one of these units are affected cannot be ascertained from our data. Dent Glasser (1979) noted, however, that in silicate minerals the stability of highly polymerized silicate polymers is lowered as the network modifier becomes smaller. It is tempting to suggest, therefore, that similar relationships may apply to melts.

The redox equilibrium in alkaline-earth metasilicates can be expressed by combining equation 1 with one that describes the redox equilibrium of iron oxides as network modifiers.

$$2Fe(VI)O_6^{9-} + 2O^-(NBO) \leftrightarrows 2Fe(VI)O_6^{10-} + O_2 \quad (4)$$

to give:

$$8Si_2O_6^{4-} + 4Fe(VI)O_6^{9-} \leftrightarrows 4SiO_4^{4-} + 6Si_2O_5^{2-} + 4Fe(VI)O_6^{10-} + O_2 \quad (5)$$

Equation 5 shows that as the degree of proportionation of the metasilicate chains increases at constant $f(O_2)$, $Fe^{3+}/\Sigma Fe$ will increase.

The equilibrium constants from equations 3 and 5 are:

$$K_1 = C^9[Fe(VI)O_6^{10-}/Fe(IV)O_2^-]^4 f(O_2) \quad (6)$$

and

$$K_2 = C[Fe(VI)O_6^{10-}/Fe(VI)O_6^{9-}]^4 f(O_2) \quad (7)$$

where

$$C = [(Si_2O_5^{2-})^6(SiO_4^{4-})^4]/Si_2O_6^{4-})^8 \quad (8)$$

Equations 6 and 7 demonstrate that the redox ratio of iron is much less sensitive to the extent of disproportionation when ferric iron is a network modifier than when it is a network former.

The value of C (eq. 8) for a given alkali metal or alkaline earth increases with increasing temperature and with decreasing pressure (Mysen *et al.*, 1980). Consequently, at constant $f(O_2)$, $Fe^{3+}/\Sigma Fe$ will increase with increasing temperature and will decrease with increasing pressure. The pressure and temperature dependence of the redox ratio is more pronounced in melts with ferric iron as a network former than in melts with ferric iron as a network modifier. The $f(O_2)$ dependence of $Fe^{3+}/\Sigma Fe$ is the same regardless of whether ferric iron is an network former or a network modifier.

Petrological applications

The above summary shows that changes of extensive and intensive variables affect physical and chemical properties of iron-bearing, rock-forming silicate melts because of the complex structural role of iron in the melts. Acidic melts such as andesite, dacite, and granite (rhyolite) will have a large excess of M^+ over M^{2+} melt modifiers. As a result, variations of redox ratios of iron will alter the degree of polymerization of the melt and therefore the viscosity and cation diffusion coefficients. It is expected, for example, that increasing $f(O_2)$ will result in increasing viscosity of the melt. Cation diffusion coefficients in silica-rich, iron-bearing melt will most likely decrease with increasing oxygen fugacity. Notably, the experimental data (Seifert *et al.*, 1979b) indicate that the activity coefficients of the Fe^{3+} and Fe^{2+} complexes do not change with oxygen fugacity. As a result, partition coefficients of ferrous and ferric iron between acidic melts and minerals in equilibrium with the melt will not be affected by the oxygen fugacity.

Physical properties of basaltic melts will be affected less by changing redox ration of iron than silica-rich melts because alteration of redox states results in smaller changes of NBO/BO. It is notable, however, that as a result of fractional crystallization of a basaltic melt to more silicic compositions, the physical properties of the magma will gradually change as the influence of redox ratios of iron on the degree of polymerization of the melt increases with increasing M^+/M^{2+}.

Acknowledgements

Critical reviews by C. M. Scarfe, H. S. Yoder, Jr., H. S. Waff, and G. Waychunas are appreciated. This research was partially supported by NSF grant EAR-7911313 and partially by the Carnegie Institution of Washington.

References

Annersten, H. and U. Hålenius (1976) Ion distribution in pink muscovite: a discussion. *Am. Mineral., 61,* 1045–1050.

——— and M. Olesch (1978) Distribution of ferrous and ferric iron in clintonite and the Mössbauer characteristics of ferric iron in tetrahedral coordination. *Can. Mineral., 16,* 199–204.

Bancroft, G. M. and R. G. Burns (1969) Mössbauer absorption spectral study of alkali amphiboles. *Mineral. Soc. Am. Spec. Pap., 2,* 137–151.

———, P. G. L. Williams and E. J. Essene (1969) Mössbauer spectra of omphacite. *Mineral Soc. Am. Spec. Pap., 2,* 59–67.

Bates, J. B., R. W. Hendricks and L. B. Shaffer (1974) Neutron irradiation effects and structure of non-crystalline SiO_2. *J. Chem. Phys., 61,* 4163–4176.

Bell, P. M. and H. K. Mao (1974) Crystal-field spectra of Fe^{2+} and Fe^{3+} in synthetic basalt glass as a function of oxygen fugacity. *Carnegie Inst. Wash. Year Book, 73,* 496–497.

Bhargava, S. C., J. E. Knudsen and S. Mørup (1979) Mössbauer study of spin–spin relaxation of Fe^{3+} ions in the presence of other paramagnetic ions. *J. Phys. Chem. Solids, 40,* 45–53.

Bockris, J. O'M. and A. K. N. Reddy (1970) *Modern Electrochemistry, Vol. 1.* Plenum Press, New York.

Bowen, N. L., J. F. Schairer and H. W. V. Willems (1930) The ternary system Na_2SiO_3–Fe_2O_3–SiO_2. *Am. J. Sci., 20,* 405–455.

Brawer, S. A. (1975) Theory of the vibrational spectra of some network and molecular glasses. *Phys. Rev. B., 11,* 3173–3194.

——— and W. B. White (1975) Raman spectroscopic investigation of the structure of silicate glasses. I. The binary silicate glasses. *J. Chem. Phys., 63,* 2421–2432.

——— and ——— (1977) Raman spectroscopic study of the structure of silicate glasses. II. Soda-alkali earth-alumina ternary and quaternary glasses. *J. Non-Cryst. Solids, 23,* 261–278.

Brown, G. E., K. D. Keefer and P. M. Fenn (1978) Extended X-ray fine structure (EXAFS) study of iron-bearing silicate glass (abstr.). *Geol. Soc. Am. Abstracts with Programs, 10,* 373.

Buddington, A. F. and D. H. Lindsley (1964) Iron–titanium oxide minerals and synthetic equivalents. *J. Petrol., 5,* 310–357.

Carmichael, I. S. E. (1967) The iron–titanium oxides of salic volcanic rocks and their associated ferromagnesian silicates. *Contrib. Mineral. Petrol., 14,* 36–64.

Dent Glasser, L. S. (1979) Non-existent silicates. *Z. Kristallogr., 149,* 291–305.

Etchepare, J. (1972) Study by Raman spectroscopy of crystalline and glassy diopside. In R. W. Douglas and B. Ellis, Eds., *Amorphous Materials,* p. 337–346. Wiley, New York.

Fudali, R. F. (1965) Oxygen fugacity of basaltic and andesitic magmas. *Geochim. Cosmochim. Acta, 29,* 1063–1075.

Furukawa, T. and W. B. White (1980) Raman spectroscopic investigation of the structure of silicate glasses. III. Alkali–silica–germanates. *J. Chem. Phys.,* in press.

———, S. A. Brawer and W. B. White (1978) The structure of lead silicate glasses determined by vibrational spectroscopy. *J. Mater. Sci., 13,* 268–282.

Kracek, F. C. (1930) The system sodium oxide–silica. *J. Phys. Chem., 34,* 1583–1598.

Kurkjian, C. R. (1970) Mössbauer spectroscopy in inorganic glasses. *J. Non-Cryst. Solids, 3,* 157–194.

Kuroda, K. and C. Kato (1979) Trimethylsilylation of hemimorphite. *J. Nucl. Inorg. Chem., 41,* 947–951.

Lauer, H. V. (1977) Effect of glass composition on major element redox equilibria: Fe^{2+}–Fe^{3+}. *Phys. Chem. Glasses, 18,* 49–52.

——— and R. V. Morris (1977) Redox equilibria of multivalent ions in silicate glasses. *J. Am. Ceram. Soc., 60,* 443–451.

Lazarev, A. N. (1972) *Vibrational Spectra and Structure of Silicates.* Consultants Bureau, New York.

MacKenzie, J. D. (Ed.) (1960) *Modern Aspects of the Vitreous State.* Butterworth's, Washington, D. C.

Mao, H. K., D. Virgo and P. M. Bell (1973) Analytical study of the orange soil returned by the Apollo 17 astronauts. *Carnegie Inst. Wash. Year Book, 72,* 631–638.

Masson, C. R. (1977) Anionic constitution of glass-forming melts. *J. Non-Cryst. Solids, 1,* 1–42.

Mysen, B. O. and D. Virgo (1978) Influence of pressure, temperature and bulk composition on melt structures in the system $NaAlSi_2O_6$–$NaFe^{3+}Si_2O_6$. *Am. J. Sci., 278,* 1307–1322.

———, ——— and F. Seifert (1979) Redox equilibria and melt structure in the system CaO–MgO–FeO–Fe_2O_3–SiO_2. *Carnegie Inst. Wash. Year Book, 78,* 519–526.

———, ——— and C. M. Scarfe (1980) Relations between anionic structure and viscosity of silicate melts—a Raman spectroscopic study at 1 atmosphere and at high pressure. *Am. Mineral. 65,* 690–710.

Osborn, E. F. (1959) Role of oxygen pressure in the crystallization and differentiation of basaltic magmas. *Am. J. Sci., 257,* 609–647.

——— (1962) Reaction series for subalkaline igneous rocks based on different oxygen pressure conditions. *Am. Mineral., 47,* 211–226.

——— (1977) Origin of calc-alkali magma series of Santorini volcano type in light of recent experimental phase-equilibrium studies. *Proceedings of the International Congress on Thermal Waters, Geothermal Energy and Vulcanism of the Mediterranean Area, Athens, October 1976, 3,* 154–167.

Roeder, P. L. and R. F. Emslie (1970) Olivine–liquid equilibrium. *Contrib. Mineral. Petrol., 29,* 275–289.

Schreiber, H. D., T. Thanyashiri, J. J. Lach and R. A. Legere (1978) Redox equilibria of Ti, Cr and Eu in silicate melts: reduction potentials and mutual interactions. *Phys. Chem. Glasses, 19,* 126–140.

Seifert, F. and M. Olesch (1977) Mössbauer spectroscopy of grandidierite, $(Mg,Fe)Al_3BSiO_9$. *Am. Mineral., 62,* 547–553.

———, D. Virgo and B. O. Mysen (1979a) Sodium loss from sodium metasilicate melts in CO_2 and CO atmospheres. *Carnegie Inst. Wash. Year Book, 78,* 679.

———, ——— and ——— (1979b) Melt structures and redox equilibria in the system Na_2O–FeO–Fe_2O_3–Al_2O_3–SiO_2. *Carnegie Inst. Wash. Year Book, 78,* 511–519.

Sharma, S. K. and H. S. Yoder (1979) Structural study of glasses of akermannite, diopside and sodium melilite compositions by Raman spectroscopy. *Carnegie Inst. Wash. Year Book, 78,* 526–532.

Taneja, S. P., C. W. Kimball and J. C. Schaffer (1973) Mössbauer spectroscopy of amorphous semiconductors and glasses containing antimony, tin and iron: a review. *Mössbauer Effect Methodology, 8,* 41–69.

Verweij, H. (1979a) Raman study of the structure of alkali germanosilicate glasses. I. Sodium and potassium metagermanosilicate glasses. *J. Non-Cryst. Solids, 33,* 41–53.

——— (1979b) Raman study of the structure of alkaligermanosilicate glasses. II. Lithium, sodium and potassium digermanosilicate glasses. *J. Non-Cryst. Solids, 33,* 55–69.

——— and W. L. Konijnendijk (1976) Structural units in K_2O–PbO–SiO_2 glasses by Raman spectroscopy. *J. Am. Ceram. Soc., 59,* 517–521.

Virgo, D., B. O. Mysen and I. Kushiro (1980) Anionic constitution of silicate melts quenched from 1 atm from Raman spectroscopy: implications for the structure of igneous melts. *Science,* in press.

———, F. Seifert and B. O. Mysen (1979) Three-dimensional network structures of melts in the systems $CaAl_2O_4$–SiO_2, $NaAlO_2$–SiO_2, $NaFeO_2$–SiO_2 and $NaGaO_2$–SiO_2 at 1 atm. *Carnegie Inst. Wash. Year Book, 78,* 506–511.

Waff, H. S. (1977) The structural role of ferric iron in silicate melts. *Can. Mineral., 15,* 198–199.

Manuscript received, September 28, 1979;
accepted for publication, May 2, 1980.